nature physics

REVIEW ARTICLE

PUBLISHED ONLINE: 31 JANUARY 2014 | DOI: 10.1038/NPHYS2877

What drives nematic order in iron-based superconductors?

R. M. Fernandes[1]*, A. V. Chubukov[2]* and J. Schmalian[3]*

Although the existence of nematic order in iron-based superconductors is now a well-established experimental fact, its origin remains controversial. Nematic order breaks the discrete lattice rotational symmetry by making the *x* and *y* directions in the iron plane non-equivalent. This can happen because of a regular structural transition or as the result of an electronically driven instability — in particular, orbital order or spin-driven Ising-nematic order. The latter is a magnetic state that breaks rotational symmetry but preserves time-reversal symmetry. Symmetry dictates that the development of one of these orders immediately induces the other two, making the origin of nematicity a physics realization of the 'chicken and egg problem'. In this Review, we argue that the evidence strongly points to an electronic mechanism of nematicity, placing nematic order in the class of correlation-driven electronic instabilities, like superconductivity and density-wave transitions. We discuss different microscopic models for nematicity and link them to the properties of the magnetic and superconducting states, providing a unified perspective on the phase diagram of the iron pnictides.

The discovery of iron-based superconductors (FeSCs) with transition temperatures T_c as high as 65 K has signalled the beginning of a new era in the investigation of unconventional superconductivity (for a review, see ref. 1). A key first step to unveil the nature of the superconducting phase is to understand the normal state from which superconductivity arises. In most FeSCs, superconductivity is found in the proximity of a magnetically ordered state (transition temperature T_{mag}), which led early on to the proposal that magnetic fluctuations play the key role in promoting the superconducting pairing[2,3]. A more careful examination of the phase diagram, however, revealed that there is another non-superconducting ordered state besides magnetism. Namely, at a certain temperature T_{nem}, the system spontaneously breaks the symmetry between the x and y directions in the Fe-plane, reducing the rotational point group symmetry of the lattice from tetragonal to orthorhombic, whereas time-reversal symmetry is preserved. In some materials, such as hole-doped $(Ba_{1-x}K_x)Fe_2As_2$, the tetragonal-to-orthorhombic and magnetic transitions are simultaneous and first-order ($T_{nem} = T_{mag}$; ref. 4), whereas in electron-doped $Ba(Fe_{1-x}Co_x)_2As_2$ and isovalent-doped $BaFe_2(As_{1-x}P_x)_2$, they are split ($T_{nem} > T_{mag}$) and, with the exception of a very small Co concentration, second order[5–8] (Fig. 1). As doping increases, the T_{nem} line tracks the T_{mag} line across the phase diagram, approaching the superconducting dome. It is therefore essential to understand the origin of this new order as it may either support or act detrimentally to superconductivity.

The order parameter for a transition in which a rotational symmetry is broken but time-reversal symmetry is preserved is a director (it defines an axis but has no sense of direction), similar to the order parameter in the nematic phase of liquid crystals[9]. By analogy, the orthorhombic state in FeSCs has been called a 'nematic state'. Unlike isotropic liquid crystals, however, in FeSCs the lattice symmetry forces the director to point only either along x or y directions. This makes the nematic order parameter Ising-like, hence the name Ising-nematic order.

At first sight, one might view this tetragonal-to-orthorhombic transition as a regular structural transition driven by lattice vibrations (phonons). However, early theoretical work[10–12] suggested that the tetragonal-to-orthorhombic transition may be driven by electronic rather than lattice degrees of freedom. Indeed, experiments find anisotropies in several electronic properties, such as the d.c. resistivity[13,14], to be much larger than the anisotropy of the lattice parameters. If the transition at T_{nem} is of electronic origin, then it is probably driven by the same fluctuations that give rise to superconductivity and magnetic order, and therefore is an integral part of a global phase diagram of FeSCs. Electronic nematic phases have recently been proposed in other unconventional superconductors, such as high-T_c cuprates and heavy-fermion materials[9]. An electronically driven nematic state in FeSCs would be in line with a generic reasoning that the pairing in all these correlated electron systems has the same origin.

The discussion on the 'nematicity' in FeSCs has been largely focused on two key issues. First, can the experiments distinguish 'beyond reasonable doubt' between phonon-driven and electron-driven tetragonal symmetry breaking? Second, if this transition is driven by electrons, which of their collective degrees of freedom is driving it — charge/orbital fluctuations or spin fluctuations? We argue below that answering the last question is crucial for the understanding of superconductivity in FeSCs, as charge/orbital fluctuations favour a sign-preserving s-wave state (s^{++}) whereas spin fluctuations favour a sign-changing s-wave (s^{+-}) or a d-wave state.

Phenomenology of the nematic phase

To describe the nematic state, the first task is to identify the appropriate order parameter. The experimental manifestations of nematic order can be clustered into three classes. Taken alone, each

[1]School of Physics and Astronomy, University of Minnesota, Minneapolis, Minnesota 55455, USA, [2]Department of Physics, University of Wisconsin-Madison, Madison, Wisconsin 53706, USA, [3]Institut für Theorie der Kondensierten Materie, und Institut für Festkörperphysik, Karlsruher Institut für Technologie, Karlsruhe D-76131, Germany. *email: rfernand@umn.edu; chubukov@physics.wisc.edu; joerg.schmalian@kit.edu

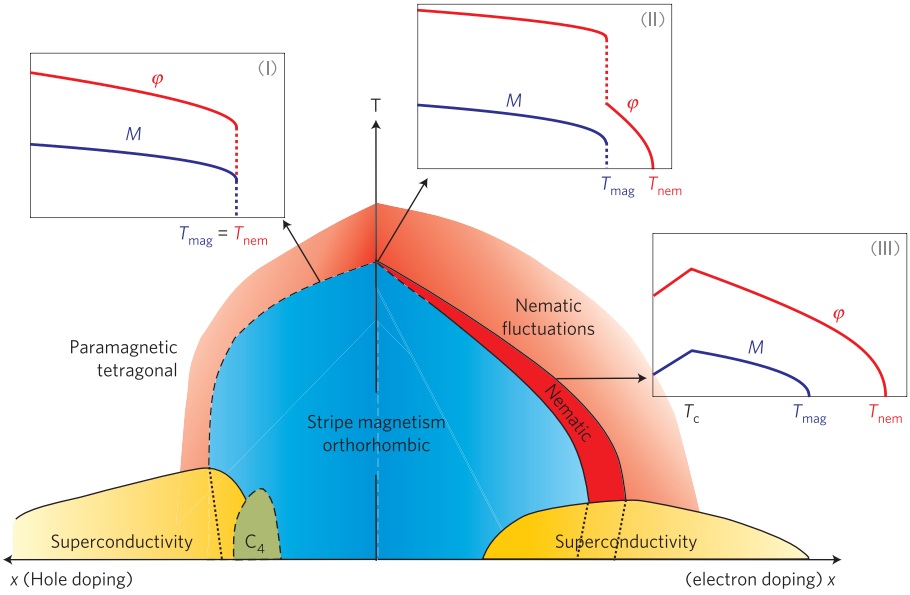

Figure 1 | Schematic phase diagram of hole-doped and electron-doped iron pnictides of the $BaFe_2As_2$ family. The blue area denotes stripe-type orthorhombic magnetism, the red area denotes nematic/orthorhombic paramagnetic order, and the yellow area superconductivity. The green area corresponds to a magnetically ordered state that preserves tetragonal (C_4) symmetry, as observed recently [56]. The dark red region denotes a regime with strong nematic fluctuations. Dotted lines illustrate the magnetic and nematic transition lines inside the superconducting dome [73]. Second-order (first-order) transitions are denoted by solid (dashed) lines. The insets show the temperature-dependence of the nematic (φ) and magnetic (M) order parameters in different regions of the phase diagram: region (I) corresponds to simultaneous first-order magnetic and nematic transitions; region (II) corresponds to split second-order nematic and first-order magnetic transitions; and region (III) corresponds to split second-order transitions. At $x = 0$ the transitions are split, like in region (II), but their separation is small [5,6].

class points to a different origin of the nematic phase (see Fig. 2 for a schematic representation):

- Structural distortion: the lattice parameters a and b along the x and y directions become different [5]. Such an order is normally associated with a phonon-driven structural transition.
- Charge/orbital order: the occupations n_{xz} and n_{yz} (and on-site energies) of the d_{xz} and d_{yz} Fe-orbitals become different [15]. The appearance of such an order is normally associated with divergent charge fluctuations.
- Spin order: the static spin susceptibility $\chi_{\rm mag}(\mathbf{q})$ becomes different along the q_x and q_y directions of the Brillouin zone before a conventional SDW state develops [7]. The appearance of such an order is normally associated with divergent quadrupole magnetic fluctuations.

The fact that these three order parameters are non-zero in the nematic phase leads to a dilemma, which can be best characterized as a physics realization of the 'chicken and egg problem': all three types of order (structural, orbital and spin-driven nematic) must be present no matter which drives the nematic instability. This follows from the fact that bi-linear combinations of the order parameters that break the same symmetry (in our case, the tetragonal symmetry of the system) are invariant under symmetry transformations and must therefore appear in the Landau free energy. Suppose that one of the three order parameters is the primary one — that is, its fluctuations drive the nematic instability. Let us call it ψ_1 and the other two ψ_2 and ψ_3, respectively. The free energy has the generic form

$$F[\psi_1,\psi_2,\psi_3] = \frac{1}{2}\chi_1^{-1}\psi_1^2 + \frac{b}{4}\psi_1^4 + \lambda_{12}\psi_1\psi_2 + \frac{1}{2}\chi_2^{-1}\psi_2^2 + \lambda_{13}\psi_1\psi_3 + \frac{1}{2}\chi_3^{-1}\psi_3^2 + \cdots \quad (1)$$

Because the transition is driven by ψ_1, the coefficient χ_1^{-1}, which, above $T_{\rm nem}$, corresponds to the inverse susceptibility of this order parameter, vanishes at $T = T_{\rm nem}$ and becomes negative for $T < T_{\rm nem}$, whereas χ_2 and χ_3 remain finite and positive (although fluctuations of ψ_2 and ψ_3 may shift $T_{\rm nem}$ slightly). For $T < T_{\rm nem}$, ψ_1 orders on its own: $\langle\psi_1\rangle = \pm(-\chi_1^{-1}/b)^{1/2}$. If the coupling constants λ_{ij} in equation (1) were zero, the other two fields ψ_2 and ψ_3 would not order, but once the λ_{ij} are finite, a non-zero $\langle\psi_1\rangle$ instantly induces finite values of the secondary order parameters $\langle\psi_2\rangle = -\lambda_{12}\chi_2\langle\psi_1\rangle$, $\langle\psi_3\rangle = -\lambda_{13}\chi_3\langle\psi_1\rangle$. As a consequence, there is only one nematic transition temperature at which all three $\langle\psi_i\rangle$ become non-zero (for example, the lattice symmetry is broken at the same temperature at which electronic nematic order emerges). Thus, it is not possible to determine which causes the instability by looking solely at equilibrium order parameters. A further experimental complication is the presence of nematic twin domains below $T_{\rm nem}$, which effectively averages $\langle\psi_1\rangle$ to zero. This problem can be circumvented by applying a small detwinning uniaxial stress [13,14], which acts as a conjugate field to ψ_1 and breaks the tetragonal symmetry at all temperatures, similar to an external magnetic field applied on a ferromagnet.

One way to select the primary order is to carefully study fluctuations in the symmetry-unbroken phase at $T > T_{\rm nem}$. Because the primary order parameter ψ_1 acts as an external field for the secondary order parameters, ψ_2 and ψ_3, fluctuations of the former renormalize the susceptibilities of the latter. For small $\lambda_{1i}\chi_i \ll 1$ $(i=2,3)$ we have

$$\tilde{\chi}_2 \approx \chi_2\left(1+\lambda_{12}^2\chi_2\chi_1\right), \quad \tilde{\chi}_3 \approx \chi_3\left(1+\lambda_{13}^2\chi_3\chi_1\right) \quad (2)$$

where $\chi_1 = \langle\psi_1^2\rangle$ is the susceptibility of the primary field. The renormalized susceptibilities of the secondary fields do diverge at the nematic transition, however, for small enough λ_{12} and λ_{13}, $\tilde{\chi}_2$ and $\tilde{\chi}_3$ begin to grow only in the immediate vicinity of $T_{\rm nem}$, where χ_1 is already large. If one can measure the three susceptibilities

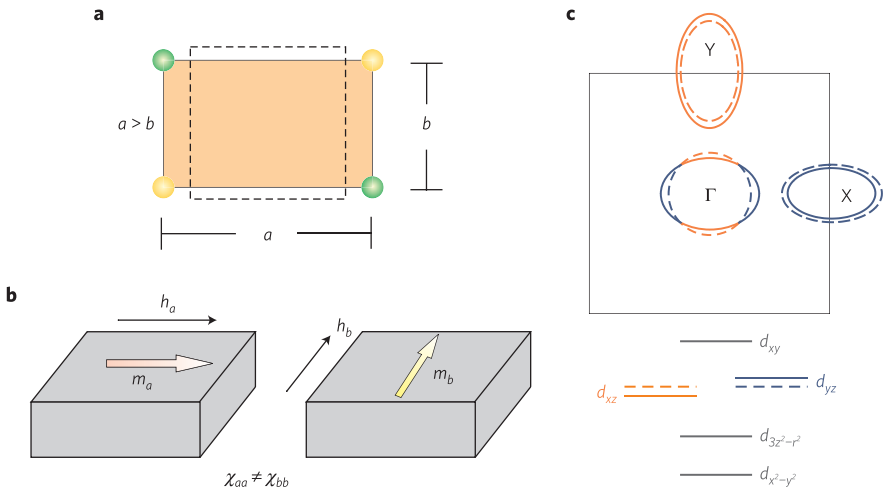

Figure 2 | Manifestations of nematic order in the iron pnictides. a, Structural distortion from a tetragonal (dashed line) to an orthorhombic (solid line) unit cell [5]. **b**, Anisotropy in the uniform spin susceptibility $\chi_{ij} = m_i/h_j$, where m_i denotes the magnetization along the i direction induced by a magnetic field h_j applied along the j direction [7]. **c**, Splitting of the d_{xz} and d_{yz} orbitals (orange and blue lines, respectively) [15]. The corresponding distortion of the Fermi surface is also shown (see also Fig. 5a).

independently, equation (2) in principle provides a criterion to decide which order parameter drives the instability. Implementation of this procedure is possible, as we shall see, but is complicated by two factors. First, it only works if λ_{12} and λ_{13} are relatively weak — that is, it depends on material-specific details. If the coupling is large, all three order parameters become so inter-connected that the question 'what is in the driver's seat?' becomes meaningless. Second, in some FeSCs the nematic transition is first order, in which case all three susceptibilities jump from one finite value to another, even before the susceptibility of the primary field gets enhanced.

Experimental evidence for electronic nematicity

We discuss separately measurements in the nematic phase and in the tetragonal phase.

Measurements in the nematic phase. The first experimental evidence for the electronic character of the tetragonal-to-orthorhombic transition came from resistivity anisotropy measurements — initially in samples partially detwinned by external magnetic fields [16] and later in samples completely detwinned by external stress [13,14]. The latter revealed that resistivity anisotropies are significantly larger than relative lattice distortions and also exhibit a non-trivial dependence on doping and disorder [17]. Other non-equilibrium quantities, such as thermopower [18] and optical conductivity [19,20], were also found to exhibit large anisotropies, which in optical measurements were observed to extend to energies of several hundreds of meV. Anisotropies in observables related to charge and spin were also seen (Fig. 2): angle-resolved photoemission spectroscopy (ARPES) found a splitting between the on-site energies of the d_{xz} and d_{yz} orbitals, indicative of orbital order [15], while torque magnetometry [7] revealed the difference between the uniform magnetic susceptibilities χ_{xx} and χ_{yy}. The latter originates from nematic order in the spin degrees of freedom, but also requires spin–orbit interaction to couple the rotational symmetry breaking in real space with the breaking of spin-rotational symmetry [21,22]. The observed onset of magnetic anisotropy in ref. 7 coincides with the observation of a non-zero orthorhombic distortion, in agreement with the earlier discussions. Strong signatures of emerging magnetic anisotropy were also found in the behaviour of the NMR lines across T_{nem} (ref. 23) and in the enhancement of the magnetic transition temperature with applied strain [24,25].

Direct observation of an electronic anisotropy in the nematic state was made possible by scanning tunnelling microscopy. The first measurements, performed deep inside the magnetic phase, found that the local density of states around an impurity is characterized by a dimer-like structure extended along the magnetic ordering vector direction [26]. Subsequent measurements showed that these dimers persist above T_{mag}, in the temperature regime of the nematic state [27]. A further piece of evidence in favour of the electronic character of the nematic transition came, ironically, from X-ray measurements of the orthorhombic distortion inside the superconducting phase. These measurements revealed a strong suppression of the distortion below T_c (ref. 28). This is a characteristic signature of the competition for the same electronic states between two electronically driven orders.

Measurements in the tetragonal phase. A few recent measurements have focused on fluctuations in the tetragonal state, in particular, on the shear modulus C_s, which is the inverse susceptibility of the structural order parameter [29–31]. If the structural transition is driven not by the lattice but by some other electronic degree of freedom, equation (2) provides a natural way to connect the shear modulus to the electronic nematic susceptibility χ_1. An experimentally observed softening of the shear modulus in a wide temperature range above T_{nem} was successfully fitted by equation (2) using both magnetic [29] and charge/orbital [30] phenomenological models for χ_1, indicating that strong lattice softening is fully consistent with electronically driven nematicity. The observation of an enhanced quasi-elastic peak in the B_{1g} Raman spectrum near T_{nem} has also been interpreted as evidence for electronic nematicity [32].

Perhaps the strongest evidence that the nematic transition is electronically driven came from recent measurements of the anisotropy of the resistivity [33]. Using a piezoelectric actuator, the measurements were performed by using strain (the structural distortion) as the control parameter, rather than stress, as in previous set-ups. Strain δ is one of the order parameter fields in the free energy equation (1). Using the resistivity anisotropy $\rho_{anis} = \rho_{xx} - \rho_{yy}$ as a proxy of the nematic order parameter, it was experimentally shown that the susceptibility $\partial\rho_{anis}/\partial\delta$ diverges near the nematic transition. This is only possible if the structural distortion is a conjugate field to the primary order parameter, rather than the primary order parameter itself — otherwise ρ_{anis} would

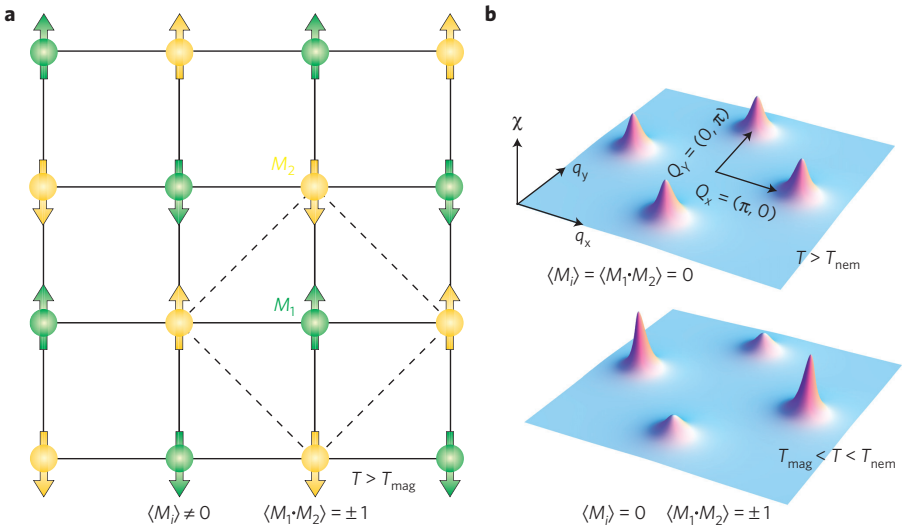

Figure 3 | Nematic order in both real and momentum space. a, Stripe magnetic configuration in real space, which can be interpreted as two inter-penetrating Néel sublattices (green and yellow) with staggered magnetization $\mathbf{M}_1$ and $\mathbf{M}_2$. In terms of the two magnetic order parameters $\mathbf{M}_X$ and $\mathbf{M}_Y$, defined in momentum space and used throughout the text, we have $\mathbf{M}_{1,2} = \mathbf{M}_X \pm \mathbf{M}_Y$. **b**, Onset of nematic order in the paramagnetic phase ($\langle \mathbf{M}_i \rangle = 0$), in terms of the magnetic susceptibility $\chi(\mathbf{q})$ across the first Brillouin zone. For $T > T_{nem}$, the two inelastic peaks at $\mathbf{Q}_X = (\pi, 0)$ and $\mathbf{Q}_Y = (0, \pi)$ have equal amplitudes — that is, $\langle M_X^2 - M_Y^2 \rangle \equiv \langle \mathbf{M}_1 \cdot \mathbf{M}_2 \rangle = 0$. For $T_{mag} < T < T_{nem}$, one of the peaks becomes stronger than the other — that is, $\langle M_X^2 - M_Y^2 \rangle \equiv \langle \mathbf{M}_1 \cdot \mathbf{M}_2 \rangle \neq 0$, which breaks the equivalence between the *x* and *y* directions.

be simply proportional to the order parameter δ, with a constant prefactor.

Microscopic models for electronic nematicity

A successful microscopic theory for electronic nematicity must describe the global phase diagram of FeSCs — that is, not only nematic order but also magnetism and superconductivity. A popular starting point is the multi-orbital Hubbard model, which describes hopping between all Fe–As orbitals and local interactions, such as intra-band and inter-band Hubbard repulsions and Hund's exchange[2]. There is general agreement among researchers that this model contains the key information about the phase diagram. The model has been analysed within an itinerant approach[34], and also assuming that electrons on at least some orbitals are localized or 'almost localized' (refs 10,11). Nematic order has been obtained in both limits, which is yet another indication that it is a generic property of FeSCs.

Whether an itinerant or a localized approach is better suited to describe magnetism and nematic order is a subtle issue. On the one hand, FeSCs are metals — that is, at low energies carriers have an itinerant character. On the other hand, the fermionic bandwidth is renormalized compared with first-principles calculations[35,36]. In some materials the renormalization is particularly strong and the magnetic susceptibility shows a Curie–Weiss behaviour over a substantial T range[37]. In this situation, the proper choice of approach is, quite possibly, material-dependent. To proceed, we adopt the itinerant scenario, where the low-energy electronic states lie around hole-like Fermi-surface pockets at the centre of the Fe-square lattice Brillouin zone and electron-like Fermi-surface pockets at the borders of the Brillouin zone, see Fig. 5a. The microscopic reasoning for either magnetic or orbital scenarios of electronic nematicity follows from two different assumptions about the sign of the effective inter-pocket interaction V_{inter}, which is a combination of the Hubbard and Hund interactions dressed up by coherence factors associated with the transformation from the orbital to the band basis[38,39]. As we will see, each scenario leads to a prediction of a particular superconducting pairing state.

Magnetic scenario. The magnetic mechanism for the nematic order follows from the observation that in most FeSCs the observed magnetic order on the Fe atoms is of the stripe type, with ordering vectors $\mathbf{Q}_X = (\pi, 0)$ or $\mathbf{Q}_Y = (0, \pi)$ — that is, spins are parallel to each other along one direction and anti-parallel along the other[40] (Fig. 3a). This order breaks not only the $O(3)$ spin-rotational symmetry (and time-reversal symmetry), but it also breaks the 90° lattice rotational symmetry down to 180° by choosing the ordering vector to be either $\mathbf{Q}_X$ or $\mathbf{Q}_Y$. This extra tetragonal symmetry breaking enhances the order parameter manifold to $O(3) \times Z_2$ (refs 10,11). In terms of the two magnetic order parameters $\mathbf{M}_X = \sum_k c^\dagger_{\mathbf{k}+\mathbf{Q}_X,\alpha} \boldsymbol{\sigma}_{\alpha\beta} c_{\mathbf{k},\beta}$ and $\mathbf{M}_Y = \sum_k c^\dagger_{\mathbf{k}+\mathbf{Q}_Y,\alpha} \boldsymbol{\sigma}_{\alpha\beta} c_{\mathbf{k},\beta}$, associated with the ordering vectors $\mathbf{Q}_X$ and $\mathbf{Q}_Y$, the breaking of the $O(3)$ symmetry implies $\langle \mathbf{M}_i \rangle \neq 0$ while the breaking of the Z_2 symmetry implies $\langle M_X^2 \rangle \neq \langle M_Y^2 \rangle$ (ref. 34). In a mean-field approach both $O(3)$ and Z_2 symmetries are broken simultaneously at T_{mag}. However, fluctuations split the two transitions and give rise to an intermediate phase at $T_{mag} < T < T_{nem}$, where the tetragonal symmetry is broken but the spin-rotational $O(3)$ symmetry is not — that is, $\langle M_X^2 \rangle \neq \langle M_Y^2 \rangle$ while $\langle \mathbf{M}_i \rangle = 0$. This is by definition a nematic order, which, viewed this way, is an unconventional magnetic order which preserves time-reversal symmetry. In real space, the stripe magnetic state can be viewed as two inter-penetrating Néel sublattices with staggered magnetizations $\mathbf{M}_1 = \mathbf{M}_X + \mathbf{M}_Y$ and $\mathbf{M}_2 = \mathbf{M}_X - \mathbf{M}_Y$. In terms of these quantities, the nematic state is characterized by the order-parameter $\psi_1 = \langle \mathbf{M}_1 \cdot \mathbf{M}_2 \rangle \neq 0$, while $\langle \mathbf{M}_i \rangle = 0$ (Fig. 3).

Within a microscopic description, the instability towards a stripe magnetic order via a second-order phase-transition is associated with the divergence of the static spin susceptibility $\chi_{mag}(\mathbf{q})$. Without any interactions, the bare particle–hole susceptibility $\chi_0(\mathbf{q})$ is by itself sizeable at $\mathbf{Q}_X$ and $\mathbf{Q}_Y$ because these wave-vectors connect electronic states at the hole and electron pockets. To be more specific, $\chi_0(\mathbf{Q}_{X,Y})$ predominantly comes from fermions with energies of the order of the bandwidth and does not change much as a function of the pocket size. When the inter-pocket interaction V_{inter} is positive (repulsive), there is an additional RPA-type enhancement of the spin susceptibility, roughly as $\chi_{mag}(\mathbf{q}) = \chi_0(\mathbf{q})/(1 - V_{inter}\chi_0(\mathbf{q}))$, and at some $T = T_{mag}$, $\chi_{mag}(\mathbf{Q}_{X,Y})$

diverges. This, however, does not guarantee that the magnetic order is of the stripe type, as the latter emerges only if below T_{mag} $\langle \mathbf{M}_X \rangle \neq 0$ and $\langle \mathbf{M}_Y \rangle = 0$, or vice versa. To determine which magnetic state develops, one needs to calculate higher-order terms in the magnetic free energy[34,39,41]. The result is that at least for small dopings, the system selects the stripe order. The static nematic susceptibility χ_{nem} (the correlator of $M_X^2 - M_Y^2$) can be obtained by including fluctuations of the nematic order parameter $M_X^2 - M_Y^2$, yielding:

$$\chi_{nem} = \frac{T \sum_q \chi_{mag}^2(\mathbf{q})}{1 - g\, T \sum_q \chi_{mag}^2(\mathbf{q})} \qquad (3)$$

where T is the temperature, and $g \propto V_{inter}^2$ is the composite coupling, which, when positive, sets the magnetic order to be of the stripe type. In dimensions $d \leq 4$, $\sum_{\mathbf{q}} \chi_{mag}^2(\mathbf{q})$ diverges at T_{mag} (assuming that the magnetic transition is second order). Equation (3) then shows that the nematic susceptibility diverges at a higher $T_{nem} > T_{mag}$, when $g \sum_{\mathbf{q}} \chi_{mag}^2(\mathbf{q}) = 1$ — that is, at sufficiently large but still finite magnetic correlation length. Equation (3) is not limited to the itinerant approach employed here and emerges in a similar fashion from any model of stripe-type magnetism, the only difference being the microscopic expression for the nematic coupling g. Provided that $g > 0$ the above reasoning naturally ties the nematic and magnetic transition temperatures over the entire phase diagram and without fine-tuning of parameters. This is a strong argument in favour of spin-driven nematicity. Between T_{nem} and T_{mag}, the Z_2 symmetry is broken but $O(3)$ is not — that is, $\langle M_X^2 \rangle \neq \langle M_Y^2 \rangle$ but $\langle \mathbf{M}_i \rangle = 0$. The difference between T_{nem} and T_{mag} is stronger in quasi-2D systems, where T_{mag} is further decreased by thermal fluctuations, whereas T_{nem} is less affected. More detailed microscopic calculations show that for some system parameters the nematic transition is second order, but for other input parameters it becomes first order[34]. In the latter case, a jump in the nematic order parameter induces a jump in the magnetic correlation length, which may instantaneously trigger a first-order magnetic transition. In weakly anisotropic three-dimensional systems, the joint first-order transition occurs for nearly all parameters — a behaviour rather generic to $d = 3$ (refs 10,34,42).

Regardless of the character of the transition, when the Fermi pockets are decomposed into their orbital characters, one finds within the same microscopic model that the emergence of spin-driven nematic order gives rise to orbital order $\Delta n = n_{xz} - n_{yz}$, as the electron pocket at $\mathbf{Q}_X$ has mostly d_{yz} character, whereas the electron pocket at $\mathbf{Q}_Y$ has mostly d_{xz} character. Similarly, a spin-driven nematic order induces a structural distortion $a \neq b$ (refs 43,44).

We see therefore that the repulsive inter-pocket interaction $V_{inter} > 0$ enhances spin fluctuations, which gives rise to both magnetism and nematicity. To describe the global phase diagram of FeSCs, one needs also to investigate superconductivity. Spin fluctuations peaked at $\mathbf{Q}_X$ and $\mathbf{Q}_Y$ strongly enhance inter-pocket repulsion, which becomes larger than intra-pocket repulsion. In this situation, the system is known to develop either an unconventional s^{+-} superconductivity, in which the gap functions have different signs in the hole and in the electron pockets, or a $d_{x^2-y^2}$ superconductivity[2,3]. We emphasize that spin-driven nematic order and s^{+-} superconductivity are both intrinsic consequences of the same magnetic scenario.

Other microscopic models also find nematic order in proximity to a magnetic instability. For instance, explicit evaluation of the ferro-orbital susceptibility using the multi-orbital Hubbard model finds that it is enhanced only in the presence of spin fluctuations[45], similarly to what is described by equation (3). Studies of models with both localized and itinerant orbitals also found[46–48] that the proximity to magnetism is an important ingredient for orbital order.

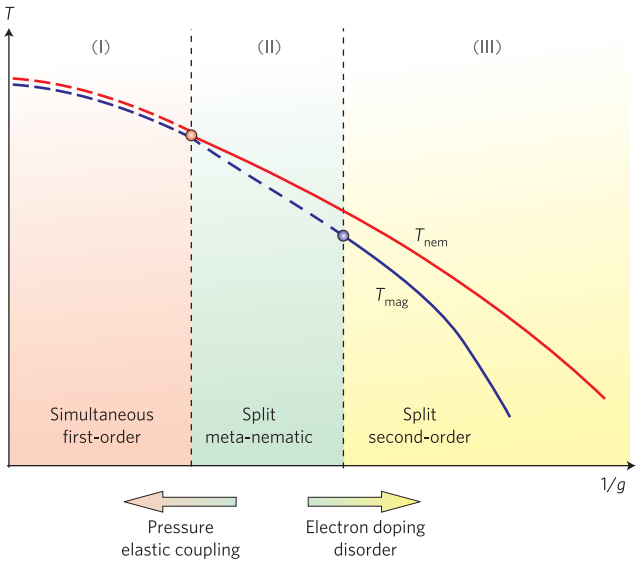

Figure 4 | Evolution of the character of the magnetic and nematic transitions in the spin-driven nematic theory. The control parameter is the inverse nematic coupling g, which changes as a function of various control parameters within an itinerant scenario (arrows). Second-order (first-order) lines are denoted by solid (dashed) lines. Regions (I)–(III) correspond to those of the phase diagram in Fig. 1. The arrows show how the nematic order parameter g is expected to evolve with doping, disorder, pressure and elastic coupling.

In purely localized-spin models the interplay between magnetism and ferro-orbital order is blurred by the complicated form of the effective Hamiltonian, which deviates from a simpler Kugel–Khomskii type[49,50].

Charge/orbital scenario. In its simplest form, the charge/orbital scenario for the nematic order parallels the magnetic scenario, the only difference being the sign of the interaction V_{inter} between electron and hole pockets. If this interaction turns out to be negative, it is the charge/orbital susceptibility rather than the spin susceptibility that is enhanced as $\chi_{orb}(\mathbf{Q}) = \chi_0(\mathbf{Q})/(1 + V_{inter}\chi_0(\mathbf{Q}))$, diverging at $\mathbf{Q}_X$ and $\mathbf{Q}_Y$ at a certain T_{orb}. This divergence would signal the onset of a charge density-wave state with ordering vectors $\mathbf{Q}_X$ or $\mathbf{Q}_Y$ (or both) and order parameters $W_X = \sum_k c^\dagger_{\mathbf{k}+\mathbf{Q}_X,\alpha}\delta_{\alpha\beta}c_{\mathbf{k},\beta}$ and $W_Y = \sum_k c^\dagger_{\mathbf{k}+\mathbf{Q}_Y,\alpha}\delta_{\alpha\beta}c_{\mathbf{k},\beta}$. This order breaks translational symmetry and, like in the magnetic scenario, breaks also an additional Z_2 symmetry if only one order parameter becomes non-zero. It is natural to expect, although no explicit calculations have been done to the best of our knowledge, that fluctuations split the temperatures at which the translational and the Z_2 symmetries are broken, in a manner similar to equation (3). Then, in the intermediate temperature range $T_{orb} < T < T_{nem}$, the system spontaneously develops an orbital order in which $\langle W_X^2 \rangle \neq \langle W_Y^2 \rangle$ while $\langle W_X \rangle = \langle W_Y \rangle = 0$. A structural distortion and the difference between $\langle M_X^2 \rangle$ and $\langle M_Y^2 \rangle$ appear instantly once orbital order sets in. However, magnetic order is not naturally linked to nematicity.

For Cooper pairing, the orbital scenario implies that the inter-pocket interaction is attractive and enhanced. Once this interaction exceeds the intra-pocket repulsion, the system develops a superconducting instability towards an s^{++} state — a conventional pairing state where the gap functions have the same sign in all pockets[3].

What we described above is one simple scenario for orbital order. Other models have also been proposed to account for the nematic

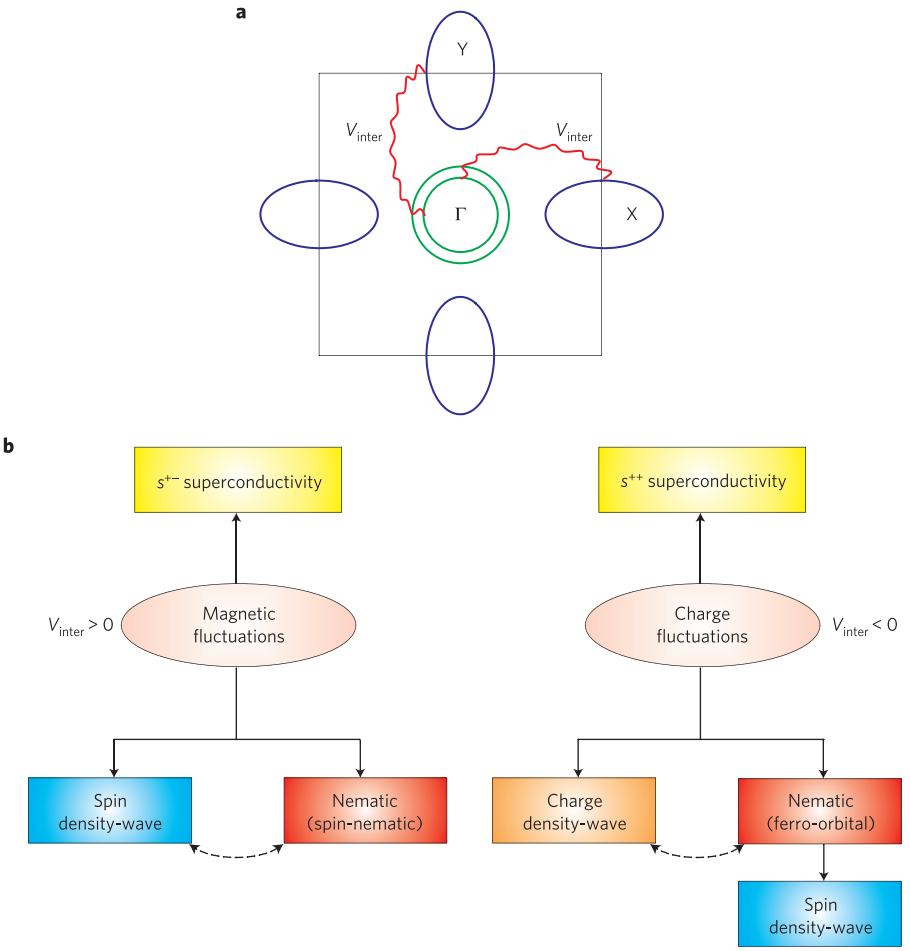

Figure 5 | Hierarchy of the electronic ordered states of FeSCs for two different types of inter-pocket interaction. **a**,The minimal Fermi surface is presented with hole pockets (green lines) at the centre (Γ) of the Fe-square lattice Brillouin zone and electron pockets (blue lines) centred at the $X = (\pi, 0)$ and $Y = (0, \pi)$ points of the Brillouin zone. V_{inter} is the inter-pocket interaction discussed in the main text. **b**, Depending on the sign of V_{inter}, either spin fluctuations ($V_{inter} > 0$, repulsion) or charge fluctuations ($V_{inter} < 0$, attraction) dominate. In the former, a stripe-type spin density-wave state is pre-empted by a spin-driven nematic phase, and the superconducting state is s^{+-} (opposite-sign gaps around the hole and electron pockets). In the latter, a stripe-type charge density-wave is pre-empted by a charge-nematic phase, and the superconducting state is s^{++} (same-sign gaps around the hole and electron pockets). In this scenario, magnetic order only appears as a secondary consequence of ferro-orbital order.

transition without involving magnetic degrees of freedom, in which a spontaneous ferro-orbital order plays the main role. In ref. 51, ferro-orbital order was proposed to develop owing to an attractive interaction involving the d_{xz} and d_{yz} orbitals. In ref. 52, it was proposed that nematicity could arise as an unequal hybridization between localized d_{xy} orbitals and itinerant d_{xz}/d_{yz} orbitals. In ref. 53 it was suggested that both spin and charge interactions are present and that the larger interaction in the spin channel gives rise to magnetic order at, say, $\mathbf{Q}_X$. However, before this happens, a weaker charge interaction gives rise to charge order at the other momentum $\mathbf{Q}_Y$ (a pocket density-wave state), which would break the tetragonal symmetry of the system. Whether such a pocket density-wave is experimentally realized in FeSCs remains to be seen.

Comparison between theory and experiment

Although the experimental evidence presented earlier favours an electronic nematic instability, disentangling the orbital and magnetic scenarios is difficult on a qualitative level, begging for a more direct comparison between microscopic models and experimental results. In this regard, the doping evolution of the magnetic and structural transitions is an important benchmark. $BaFe_2As_2$, one of the compounds most extensively investigated, exhibits a second-order nematic transition at T_{nem} followed by a first-order 'meta–nematic transition' at a lower T, where the system simultaneously undergoes a first-order magnetic transition, see inset (II) in Fig. 1. The meta–nematic transition has been observed by X-ray[5,6] and torque magnetometry[7], although the data disagree on the precise value of T_{nem}. As charge carriers are introduced in the system via Co substitution in the Fe-sites, the splitting between the two transitions increases, and eventually the meta–nematic transition disappears and the magnetic transition becomes second order as well.

How does this compare with theory? For the magnetic scenario, a detailed theoretical analysis[34] shows that three types of system behaviour are possible in systems that are moderately anisotropic, depending on the value of the nematic coupling g (Fig. 4). At large g, nematic and magnetic transitions are simultaneous and first order. At intermediate g, nematic order develops via a second-order transition, and there is a meta–nematic transition at a lower T, where magnetic order also develops discontinuously. At smaller g, nematic and magnetic transitions are separate and second order, with an intermediate Ising-nematic phase between T_{nem} and T_{mag}. The microscopic calculations found that g decreases with electron doping, and the theoretical phase diagram in Fig. 4 is fully consistent

with the one for the electron-doped $Ba(Fe_{1-x}Co_x)_2As_2$ if we place the $x = 0$ point in region (II) in Fig. 4. The splitting between the two transition temperatures for $x = 0$ is very small and can hardly be seen in Fig. 1, but is indicated in inset (II). No calculations of how the nematic and magnetic transitions evolve with carrier concentration have been done within the charge/orbital scenario.

One can take the comparison of the data even further and compare the two versions of the magnetic scenario — for itinerant and for localized spins. Both predict stripe magnetic order and pre-emptive Z_2 symmetry-breaking, but differ in the details. In particular, in localized models g is generally small and is unaffected by carrier concentration [10,12]. This makes the description of the doping dependence in the localized spin approach somewhat problematic, although not impossible [42]. A more essential difference is that in the localized J_1–J_2 model the coupling g is always positive. This follows from the principle that spins tend to align themselves perpendicular to the fluctuating Weiss field of the surrounding spins on the other sublattice [54]. In contrast, in itinerant models g becomes negative at large enough hole doping [41,55,56]. For negative g, there is no tetragonal symmetry breaking either above or below the magnetic transition, as the system selects a tetragonally symmetric combination of both $\mathbf{Q}_X$ and $\mathbf{Q}_Y$ orders. A symmetry-preserving magnetic state with ordering vectors at $\mathbf{Q}_X$ and $\mathbf{Q}_Y$ has been recently observed in $Ba_{1-x}Na_xFe_2As_2$ (ref. 56) and $Ba(Fe_{1-x}Mn_x)_2As_2$ (ref. 57) at large enough doping. In principle, one could obtain the change of sign of g by adding extra terms to the J_1–J_2 model; however, the fact that such a sign change appears naturally in the itinerant model is an argument in favour of this magnetic scenario.

Another key quantity to compare in experiment and theory is the resistivity anisotropy. Deep in the magnetically ordered state, the anisotropic folding of the Fermi surface plays the main role in determining the resistivity anisotropy [14,58]. In the nematic state, $T > T_{mag}$, orbital order and spin-driven nematic order have different effects on the d.c. resistivity: whereas the former causes an anisotropy in the Drude weight [46,59], the latter gives rise to anisotropy in the scattering rate [60]. The calculated anisotropy in the Drude weight has the opposite sign to the one observed experimentally [46,59], whereas the calculated anisotropy in the magnetic scattering rate was shown to agree with experiments, including a sign-change of the anisotropy between electron-doped and hole-doped materials [61].

One can also compare theoretical and experimental results for the feedback effects from nematic order on the electronic and the magnetic spectrum [34,46,62]. In the magnetic scenario, nematic order enhances the magnetic correlation length. This gives rise to strong magnetic fluctuations and a possible pseudogap in the electronic spectrum. A significant increase of magnetic fluctuations below T_{nem} has been observed via NMR in compounds where T_{nem} and T_{mag} are well separated [63]. Also, recent angle-resolved photoemission spectroscopy experiments found pseudogap behaviour (a suppression in the density of states at low energies) whose onset coincides with the nematic transition [64]. Within the orbital scenario, the key feedback from the orbital order is a Pomeranchuk distortion of the Fermi surface induced by orbital polarization [46].

Nematic fluctuations above T_{nem} have also been used to compare experiment and theory. Orbital fluctuations have been argued to affect the density of states at the Fermi level [65] and leave signatures in point-contact spectroscopy consistent with the data [66]. Alternatively, one can employ equation (2) to compare the renormalized lattice susceptibility (the shear modulus C_s), assumed to be non-critical, with the susceptibility χ_1 associated with either the orbital or the spin-driven nematic order parameter. Equation (2) must be satisfied if the corresponding electronic order drives the nematic instability. In ref. 32, a quasi-elastic peak in the Raman response was attributed to charge/orbital fluctuations and used to extract the corresponding orbital susceptibility. On the other hand, the nematic susceptibility in the spin-driven approach, being proportional to $\sum_{\mathbf{q}} \chi^2_{mag}(\mathbf{q})$ (see equation (3)), can be measured via the NMR spin-lattice relaxation rate $1/T_1$. Comparison with shear modulus data for a family of electron-doped FeSCs found that there is a robust scaling between C_s and $1/T_1$ data [67]. This provides strong support for the idea that the nematic transition is spin-driven.

Perspectives

The bulk of experimental and theoretical results we have presented in this short Review support the idea that nematic order in FeSCs is of electronic origin, which places it on a par with other known electronic instabilities such as superconductivity or density-wave orders. It is likely that magnetic fluctuations drive the nematic instability. In any case, all three orders — spin-driven Ising-nematic, orbital, and structural — appear simultaneously below T_{nem}. The important question not addressed until very recently is the role of nematicity for high-temperature superconductivity. It is unlikely that nematic fluctuations can mediate superconductivity as spin or charge fluctuations do, as it involves small momentum transfer, but nematic fluctuations may nevertheless enhance T_c by reducing the bare intra-pocket repulsion [21]. Intra-pocket interactions, however, in general do not select the relative sign of the gaps in different pockets. Below T_c nematic order has been found to compete with superconductivity [28,68], as density-wave orders do. A special case in which nematicity strongly affects T_c is when s-wave and d-wave superconducting instabilities are nearly degenerate, as was suggested to be the case for strongly hole-doped and strongly electron-doped FeSCs [69]. In this situation nematic order leads to a sizeable enhancement of T_c by lifting the frustration associated with the competing pairing states [70–72]. These results clearly point to the need for further investigations of the interplay between nematicity and superconductivity.

Received 17 October 2013; accepted 17 December 2013; published online 31 January 2014

References

1. Paglione, J. & Greene, R. L. High-temperature superconductivity in iron-based materials. *Nature Phys.* **6,** 645–658 (2010).
2. Hirschfeld, P. J., Korshunov, M. M. & Mazin, I. I. Gap symmetry and structure of Fe-based superconductors. *Rep. Prog. Phys.* **74,** 124508 (2011).
3. Chubukov, A. V. Pairing mechanism in Fe-based superconductors. *Annu. Rev. Condens. Matter Phys.* **3,** 57–92 (2012).
4. Avci, S. *et al.* Phase diagram of $(Ba_{1-x}K_x)Fe_2As_2$. *Phys. Rev. B* **85,** 184507 (2012).
5. Kim, M. G. *et al.* Character of the structural and magnetic phase transitions in the parent and electron-doped $BaFe_2As_2$ compounds. *Phys. Rev. B* **83,** 134522 (2011).
6. Rotundu, C. R. & Birgeneau, R. J. First- and second-order magnetic and structural transitions in $Ba(Fe_{1-x}Co_x)_2As_2$. *Phys. Rev. B* **84,** 092501 (2011).
7. Kasahara, S. *et al.* Electronic nematicity above the structural and superconducting transition in $BaFe_2(As_{1-x}P_x)_2$. *Nature* **486,** 382–385 (2012).
8. Zhou, R. *et al.* Quantum criticality in electron-doped $BaFe_{2-x}Ni_xAs_2$. *Nature Comm.* **4,** 2265 (2013).
9. Fradkin, E., Kivelson, S. A., Lawler, M. J., Eisenstein, J. P. & Mackenzie, A. P. Nematic Fermi fluids in condensed matter physics. *Annu. Rev. Condens. Matter Phys.* **1,** 153–178 (2010).
10. Fang, C., Yao, H., Tsai, W-F., Hu, J. & Kivelson, S. A. Theory of electron nematic order in LaFeAsO. *Phys. Rev. B* **77,** 224509 (2008).
11. Xu, C., Muller, M. & Sachdev, S. Ising and spin orders in the iron-based superconductors. *Phys. Rev. B* **78,** 020501(R) (2008).
12. Chandra, P., Coleman, P. & Larkin, A. I. Ising transition in frustrated Heisenberg models. *Phys. Rev. Lett.* **64,** 88–91 (1990).
13. Chu, J-H. *et al.* In-plane resistivity anisotropy in an underdoped iron arsenide superconductor. *Science* **329,** 824–826 (2010).
14. Tanatar, M. A. *et al.* Uniaxial-strain mechanical detwinning of $CaFe_2As_2$ and $BaFe_2As_2$ crystals: Optical and transport study. *Phys. Rev. B* **81,** 184508 (2010).
15. Yi, M. *et al.* Symmetry-breaking orbital anisotropy observed for detwinned $Ba(Fe_{1-x}Co_x)_2As_2$ above the spin density wave transition. *Proc. Natl Acad. Sci. USA* **108,** 6878–6883 (2011).
16. Chu, J-H *et al.* In-plane electronic anisotropy in underdoped $Ba(Fe_{1-x}Co_x)_2As_2$ revealed by partial detwinning in a magnetic field. *Phys. Rev. B* **81,** 214502 (2010).
17. Nakajima, M. *et al.* Effect of Co doping on the in-plane anisotropy in the optical spectrum of underdoped $Ba(Fe_{1-x}Co_x)_2As_2$. *Phys. Rev. Lett.* **109,** 217003 (2012).

18. Jiang, S. *et al.* Thermopower as a sensitive probe of electronic nematicity in iron pnictides. *Phys. Rev. Lett.* **110,** 067001 (2013).
19. Dusza, A. *et al.* Anisotropic charge dynamics in detwinned $Ba(Fe_{1-x}Co_x)_2As_2$. *Europhys. Lett.* **93,** 37002 (2011).
20. Nakajima, M. *et al.* Unprecedented anisotropic metallic state in undoped iron arsenide $BaFe_2As_2$ revealed by optical spectroscopy. *Proc. Natl Acad. Sci. USA* **108,** 12238–12242 (2011).
21. Fernandes, R. M. & Schmalian, J. Manifestations of nematic degrees of freedom in the magnetic, elastic, and superconducting properties of the iron pnictides. *Supercond. Sci. Technol.* **25,** 084005 (2012).
22. Cvetkovic, V. & Vafek, O. Space group symmetry, spin-orbit coupling and the low energy effective Hamiltonian for iron based superconductors. *Phys. Rev. B* **88,** 134510 (2013).
23. Fu, M. *et al.* NMR search for the spin nematic state in LaFeAsO single crystal. *Phys. Rev. Lett.* **109,** 247001 (2012).
24. Dhital, C. *et al.* Effect of uniaxial strain on the structural and magnetic phase transitions in $BaFe_2As_2$. *Phys. Rev. Lett.* **108,** 087001 (2012).
25. Hu, J., Setty, C. & Kivelson, S. Pressure effects on magnetically driven electronic nematic states in iron pnictide superconductors. *Phys. Rev. B* **85,** 100507 (2012).
26. Chuang, T-M. *et al.* Nematic electronic structure in the parent state of the iron-based superconductor $Ca(Fe_{1-x}Co_x)_2As_2$. *Science* **327,** 181–184 (2010).
27. Rosenthal, E. P. *et al.* Visualization of electron nematicity and unidirectional antiferroic fluctuations at high temperatures in NaFeAs. *Nature Phys.* http://dx.doi.org/10.1038/nphys2870 (2014) .
28. Nandi, S. *et al.* Anomalous suppression of the orthorhombic lattice distortion in superconducting $Ba(Fe_{1-x}Co_x)_2As_2$ single crystals. *Phys. Rev. Lett.* **104,** 057006 (2010).
29. Fernandes, R. M. *et al.* Effects of nematic fluctuations on the elastic properties of iron arsenide superconductors. *Phys. Rev. Lett.* **105,** 157003 (2010).
30. Yoshizawa, M. *et al.* Structural quantum criticality and superconductivity in iron-based superconductor $Ba(Fe_{1-x}Co_x)_2As_2$. *J. Phys. Soc. Jpn* **81,** 024604 (2012).
31. Böhmer, A. E. *et al.* Nematic susceptibility of hole- and electron-doped $BaFe_2As_2$ iron-based superconductors. Preprint at http://arxiv.org/abs/1305.3515 (2013) .
32. Gallais, Y. *et al.* Observation of incipient charge nematicity in $Ba(Fe_{1-x}Co_x)_2As_2$. *Phys. Rev. Lett.* **111,** 267001 (2013).
33. Chu, J-H. *et al.* Divergent nematic susceptibility in an iron arsenide superconductor. *Science* **337,** 710–712 (2012).
34. Fernandes, R. M., Chubukov, A. V., Knolle, J., Eremin, I. & Schmalian, J. Preemptive Nematic order pseudogap, and orbital order in the iron pnictides. *Phys. Rev. B* **85,** 024534 (2012).
35. Ortenzi, L., Cappelluti, E., Benfatto, L. & Pietronero, L. Fermi surface shrinking and interband coupling in iron-based pnictides. *Phys. Rev. Lett.* **103,** 046404 (2009).
36. Yin, Z. P., Haule, K. & Kotliar, G. Kinetic frustration and the nature of the magnetic and paramagnetic states in iron pnictides and iron chalcogenides. *Nature Mater.* **10,** 932–935 (2011).
37. Hardy, F. *et al.* Evidence of strong correlations and coherence-incoherence crossover in the iron pnictide superconductor KFe_2As_2. *Phys. Rev. Lett.* **111,** 027002 (2013).
38. Chubukov, A. V., Efremov, D. V. & Eremin, I. Magnetism, superconductivity, and pairing symmetry in iron-based superconductors. *Phys. Rev. B* **78,** 134512 (2008).
39. Eremin, I. & Chubukov, A. V. Magnetic degeneracy and hidden metallicity of the spin-density-wave state in ferrophictides. *Phys. Rev. B* **81,** 024511 (2010).
40. Dai, P., Hu, J. & Dagotto, E. Magnetism and its microscopic origin in iron-based high-temperature superconductors. *Nature Phys.* **8,** 709–718 (2012).
41. Brydon, P. M. R., Schmiedt, J. & Timm, C. Microscopically derived Ginzburg-Landau theory for magnetic order in the iron pnictides. *Phys. Rev. B* **84,** 214510 (2011).
42. Kamiya, Y., Kawashima, N. & Batista, C. D. Dimensional crossover in the quasi-two-dimensional Ising-O(3) model. *Phys. Rev. B* **84,** 214429 (2011).
43. Qi, Y. & Xu, C. Global phase diagram for magnetism and lattice distortion of iron-pnictide materials. *Phys. Rev. B* **80,** 094402 (2009).
44. Cano, A., Civelli, M., Eremin, I. & Paul, I. Interplay of magnetic and structural transitions in Fe-based pnictide superconductors. *Phys. Rev. B* **82,** 020408(R) (2010).
45. Onari, S. & Kontani, H. Self-consistent vertex correction analysis for iron-based superconductors: Mechanism of Coulomb interaction-driven orbital fluctuations. *Phys. Rev. Lett.* **109,** 137001 (2012).
46. Lv, W. & Phillips, P. Orbitally and magnetically induced anisotropy in iron-based superconductors. *Phys. Rev. B* **84,** 174512 (2011).
47. Liang, S., Moreo, A. & Dagotto, E. Nematic state of pnictides stabilized by interplay between spin, orbital, and lattice degrees of freedom. *Phys. Rev. Lett.* **111,** 047004 (2013).
48. Lee, C. C., Yin, W. G. & Ku, W. Ferro-orbital order and strong magnetic anisotropy in the parent compounds of iron-pnictide superconductors. *Phys. Rev. Lett.* **103,** 267001 (2009).
49. Krüger, F. S., Kumar, J., Zaanen, J. & van den Brink,Spin-orbital frustrations and anomalous metallic state in iron-pnictide superconductors. *Phys. Rev. B* **79,** 054504 (2009).
50. Applegate, R., Singh, R. R. P., Chen, C-C. & Devereaux, T. P. Phase transitions in spin-orbital models with spin-space anisotropies for iron pnictides: Monte Carlo simulations. *Phys. Rev. B* **85,** 054411 (2012).
51. Yamase, H. & Zeyher, R. Superconductivity from orbital nematic fluctuations. *Phys. Rev. B* **88,** 180502(R) (2013).
52. Stanev, V. & Littlewood, P. B. Nematicity driven by hybridization in iron-based superconductors. *Phys. Rev. B* **87,** 161122(R) (2013).
53. Kang, J. & Tesanovic, Z. Theory of the valley-density wave and hidden order in iron pnictides. *Phys. Rev. B* **83,** 020505 (2011).
54. Henley, C. L. Ordering due to disorder in a frustrated vector antiferromagnet. *Phys. Rev. Lett.* **62,** 2056–2059 (1989).
55. Lorenzana, J., Seibold, G., Ortix, C. & Grilli, M. Competing orders in FeAs layers. *Phys. Rev. Lett.* **101,** 186402 (2008).
56. Avci, S. *et al.* The origin of nematic order in the iron-based superconductors. Preprint at http://arxiv.org/abs/1303.2647 (2013) .
57. Kim, M. G. *et al.* Antiferromagnetic ordering in the absence of a structural distortion in $Ba(Fe_{1-x}Mn_x)_2As_2$. *Phys. Rev. B* **82,** 220503(R) (2010).
58. Valenzuela, B., Bascones, E. & Calderon, M. J. Conductivity anisotropy in the antiferromagnetic state of iron pnictides. *Phys. Rev. Lett.* **105,** 207202 (2010).
59. Chen, C-C., Maciejko, J., Sorini, A. P., Moritz, B., Singh, R. R. P. & Devereaux, T. P. Orbital order and spontaneous orthorhombicity in iron pnictides. *Phys. Rev. B* **82,** 100504 (2010).
60. Fernandes, R. M., Abrahams, E. & Schmalian, J. Anisotropic in-plane resistivity in the nematic phase of the iron pnictides. *Phys. Rev. Lett.* **107,** 217002 (2011).
61. Blomberg, E. C. *et al.* Sign-reversal of the in-plane resistivity anisotropy in hole-doped iron pnictides. *Nature Commun.* **4,** 1914 (2013).
62. Goswami, P., Yu, R., Si, Q. & Abrahams, E. Spin dynamics of a $J_1 - J_2$ antiferromagnet and its implications for iron pnictides. *Phys. Rev. B* **84,** 155108 (2011).
63. Ma, L. *et al.* ^{23}Na and ^{75}As NMR study of antiferromagnetism and spin fluctuations in NaFeAs single crystals. *Phys. Rev. B* **83,** 132501 (2011).
64. Shimojima, T. *et al.* Pseudogap formation above the superconducting dome in iron-pnictides. *Phys. Rev. B* **89,** 045101 (2013).
65. Lee, W-C. & Phillips, P. W. Non-Fermi liquid due to orbital fluctuations in iron pnictide superconductors. *Phys. Rev. B* **86,** 245113 (2012).
66. Arham, H. Z. *et al.* Detection of orbital fluctuations above the structural transition temperature in the iron pnictides and chalcogenides. *Phys. Rev. B* **85,** 214515 (2012).
67. Fernandes, R. M., Böhmer, A. E., Meingast, C. & Schmalian, J. Scaling between magnetic and lattice fluctuations in iron-pnictide superconductors. *Phys. Rev. Lett.* **111,** 137001 (2013).
68. Moon, E. G. & Sachdev, S. Competition between superconductivity and nematic order: Anisotropy of superconducting coherence length. *Phys. Rev. B* **85,** 184511 (2012).
69. Reid, J-Ph. *et al.* Universal heat conduction in the iron-arsenide superconductor KFe_2As_2: Evidence of a d-wave state. *Phys. Rev. Lett.* **109,** 087001 (2012).
70. Fernandes, R. M. & Millis, A. J. Nematicity as a probe of superconducting pairing in iron-based superconductors. *Phys. Rev. Lett.* **111,** 127001 (2013).
71. Livanas, G., Aperis, A., Kotetes, P. & Varelogiannis, G. Nematicity from mixed $s_{+-} + d_{x^2-y^2}$ states in iron-based superconductors. Preprint at http://arxiv.org/abs/1208.2881 (2012) .
72. Yang, F., Wang, F. & Lee, D-H. Fermiology, orbital order, orbital fluctuation and cooper pairing in iron-based superconductors. *Phys. Rev. B* **88,** 100504 (2013).
73. Fernandes, R. M., Maiti, S., Wölfle, P. & Chubukov, A. V. How many quantum phase transitions exist inside the superconducting dome of the iron pnictides?. *Phys. Rev. Lett.* **111,** 057001 (2013).

Acknowledgements

We acknowledge useful discussions with E. Abrahams, J. Analytis, E. Bascones, A. Böhmer, J. van den Brink, P. Brydon, S. Bud'ko, P. Canfield, P. Chandra, P. Dai, M. Daghofer, L. Degiorgi, I. Eremin, I. Fisher, Y. Gallais, A. Goldman, A. Kaminski, J. Kang, V. Keppens, D. Khalyavin, M. Khodas, S. Kivelson, J. Knolle, H. Kontani, A. Kreyssig, F. Krüger, W. Ku, W.C. Lee, J. Lorenzana, W. Lv, S. Maiti, D. Mandrus, R. McQueeney, Y. Matsuda, I. Mazin, C. Meingast, A. Millis, P. Orth, R. Osborn, A. Pasupathy, I. Paul, P. Phillips, R. Prozorov, S. Sachdev, Q. Si, T. Shibauchi, L. Taillefer, M. Takigawa, M. Tanatar, M. Vavilov, P. Wölfle and M. Yoshizawa. The authors benefited much from discussions with our colleague Z. Tesanovic, who unexpectedly passed away last year. A.V.C. is supported by the Office of Basic Energy Sciences US Department of Energy under the grant #DE-FG02-ER46900. J.S. is supported by the Deutsche Forschungsgemeinschaft through DFG-SPP 1458 'Hochtemperatursupraleitung in Eisenpniktiden'.

Author contributions

All authors were responsible for writing and revising the paper.

Additional information

Reprints and permissions information is available online at www.nature.com/reprints. Correspondence and requests for materials should be addressed to R.M.F., A.V.C. or J.S.

Competing financial interests

The authors declare no competing financial interests.